Progress In Electromagnetics Research, Vol. 138, 555–569, 2013

AN EXTENDED INVERSE CHIRP-Z TRANSFORM ALGORITHM TO PROCESS HIGH SQUINT SAR DATA

Yue Liu*, Yun Kai Deng, and Robert Wang

Spaceborne Microwave Remote Sensing System Department, Institute of Electronics, Chinese Academy of Sciences (IECAS), China

Abstract—This paper proposes an Extended Inverse Chirp-Z Transform (EICZT) algorithm to handle the high squint FMCW SAR data, where the conventional Inverse Chirp-Z Transform (ICZT) cannot work due to the failure in dealing with the range-variance of second- and higher-order range-azimuth coupling terms. A preprocessing operation is implemented in the azimuth-Doppler and range-time (Doppler-time) domain, where a perturbation function consisting of second-order and third-order range time variables is implemented to compensate the range variance of the second order range terms. Moreover, a new scaling factor is formulated to represent the Range Cell Migration (RCM), and further corrected by the presented EICZT approach. The proposed approach is analyzed and compared with the conventional ICZT. The simulated high squint SAR scene with nine targets is well focused by the proposed approach and the quality is greatly improved with respect the conventional ICZT. The proposed algorithm is also validated by the X-band high-resolution real SAR data.

1. INTRODUCTION

SAR systems are playing an important role in airborne and spaceborne earth observation fields, such as reconnaissance, concealed target detection, robotic sensing, nondestructive testing, gas flow measurements, mine detection, surveillance and so on [1–11]. Squint SAR has a potential to provide the information about the target through the measurement of the azimuthally angle dependence of backscatter. Squint configuration can also increase the flexibility of the planned mission with antenna which is electronically or mechanically pointed to the desirable area within a single pass of the platform [1].

Received 14 February 2013, Accepted 15 March 2013, Scheduled 4 April 2013

* Corresponding author: Yue Liu (liuyuehappy@gmail.com).

However, signal processing of high squint SAR signal is more complicated. Several algorithms are developed to process SAR signal in high squint configurations with different disadvantages. Range Doppler Algorithm (RDA) with Secondary Range Compression (SRC) [1, 12] and Wavenumber Domain Algorithm (WDA) [1, 12] are both capable of handling high squint SAR signal using interpolation operations, which increase the computational load. Moreover, the interpolation for WDA is carried out in wavenumber domain where the dependency of velocity variable on the slant range cannot be accounted. If the illuminated scene has a wide swath, e.g., in spaceborne configurations, it has to be divided into several sub-swaths, which further decreases the efficiency. Nonlinear Chirp Scaling Algorithm (NCSA) can also deal with squint signal [1, 13–16], however, NCSA is developed based on Chirp Scaling Algorithm (CSA), thus requires that the received echo signal must be in chirp modulation. But in some situations the received signal does not hold the chirp modulation, such as when dechirp-on-receive operation is applied in spotlight SAR [17] or Frequency Modulated Continous Wave (FMCW) SAR mode [18], NCSA will be completely disabled.

Chirp-Z Transform (CZT) was firstly developed by Dr. Rabiner. Investigation is then carried out using Inverse Chirp-Z Transform (ICZT) algorithm to compensate the Range Cell Migration (RCM) of SAR signal in order to achieve fine images [19–24]. Unlike the RDA and WDA, ICZT is carried out without any interpolation operations. Furthermore, different from the NCSA, which depends on the transmitted signal form, ICZT can be implemented to process the signal in any modulation, thus has a great potential in SAR applications in advanced modes, such as spotlight SAR or continuous-wave SAR systems. Nevertheless conventional ICZT algorithm is limited to handling broadside configurations or low squint configurations, because of the ignoring of the range variance of second- and higher-order range terms [19–24]. In this paper, an Extended Inverse Chirp-Z Transform (EICZT) approach is proposed with a pre-processing operation in the azimuth-Doppler and range-time (Doppler-time) domain to compensate the range variance of the second order range terms, by using a perturbation function consisting of second-order and third-order range time variables. Furthermore, a new scaling factor is formulated and corrected by the EICZT operation. Simultaneously, EICZT maintains the advantages of conventional ICZT, which does not need interpolation and is capable of dealing with signal in any modulation. Analyses are carried out about the phase error to highlight the validation and essentiality of the proposed EICZT approach. Simulation experiments and real data processing results validate that the proposed approach is feasible in high squint

configurations.

This paper is organized as follows. In Section 2, the focusing algorithm for high squint SAR data is developed based on the EICZT operation. Section 3 analyzes the phase error of proposed EICZT approach and compares it with conventional ICZT algorithm. An airborne simulation experiment in high squint mode with a squint angle of 40° is designed and the processing result of real X-band SAR data is shown in Section 4. Finally, conclusions are reported in Section 5.

2. SIGNAL PROCESSING ALGORITHM

The squint SAR geometry is shown as Figure 1 The mathematical symbols and their definitions used in this paper are listed as follows.

f, f_τ: Range and azimuth frequency variables.

λ, f_0: Carrier wavelength and frequency of the transmitted signal.

$\sigma(\tau_0, r_0)$: Backscattering coefficient of the point target $P(\tau_0, r_0)$.

τ_0: Zero-Doppler time of the target $P(\tau_0, r_0)$.

r_0: Shortest slant range of the target to the antenna.

K_r: Chirp rate.

c: Light speed.

v: Flight velocity.

The conventional ICZT is used to correct the Range Cell Migration (RCM), but neglects the range-variant effect of the second- and higher-order range terms, what is not acceptable in high squint situations [19–24]. To make the algorithm feasible in high squint configurations, a pre-processing operation is proposed to compensate the range-variance of second order range terms in the Doppler-time domain.

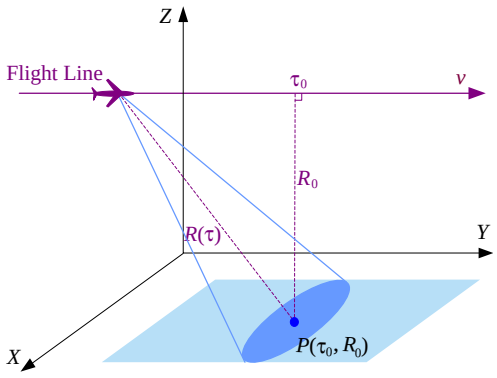

Figure 1. Squint SAR geometry.

Based on the aforementioned idea, an extended ICZT algorithm is ready to be proposed. The signal processing procedure is shown in the block diagram in Figure 2, and its basic operations are illustrated as follows.

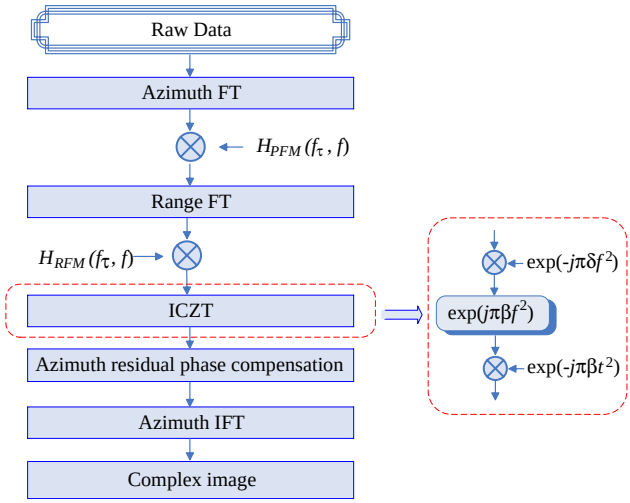

Figure 2. Signal processing procedure.

2.1. Azimuth FFT

To clearly show our processing strategy, the analytical expressions are desirable. However, the signal expression in the Doppler-time domain cannot be readily formulated by the principle of stationary phase in terms of azimuth time variable since it is involved in two square root terms [1]. Therefore, the signal expression in the azimuth-Doppler and range-time domain has to be obtained indirectly by transforming the signal from the two-dimensional (2D) frequency domain to the Doppler-time domain.

Defining the transmitted FM signal as $s(t) = \exp(j\pi K_r t^2)$, the 2D spectrum is formulated as [1]:

$$G(f_\tau, f_0) = \sigma(\tau_0, r_0) \exp[j\Phi(f_\tau, f)] \tag{1}$$

where the phase function $\Phi(f_\tau, f)$ is expressed as

$$\Phi(f_\tau, f) = -\frac{4\pi r_0}{c}\sqrt{(f_0+f)^2 - \left(\frac{cf_\tau}{2v}\right)^2} - \frac{\pi f^2}{K_r} - 2\pi f_\tau \tau_0 \tag{2}$$

The involved azimuth modulation components can be better understood by expanding the square root of (2) using a Taylor series,

i.e.,

$$\Phi(f_\tau,f)=-\frac{4\pi r_0}{c}\left[Df_0+\Phi_1(f_\tau)f+\Phi_2(f_\tau)f^2+\Phi_3(f_\tau)f^3+\ldots\right]-\frac{\pi f^2}{K_r}-2\pi f_\tau\tau_0 \quad (3)$$

where

$$\mu = \left(\frac{cf_\tau}{2vf_0}\right), \quad D=\sqrt{1-\mu^2} \quad (4)$$

$$\Phi_1(f_\tau) = \frac{1}{D}, \quad \Phi_2(f_\tau)=-\frac{\mu^2}{2f_0D^3}, \quad \Phi_3(f_\tau)=\frac{\mu^2}{2f_0^2D^5} \quad (5)$$

Keeping the phase term up to the third-order, and using the principle of stationary phase in terms of range frequency variable f in (3), the 2D spectrum is transformed to the Doppler-time domain, which is formulated as

$$G(f_\tau,t)=\sigma(\tau_0,r_0)\exp\left[j\Phi(f_\tau,t)\right] \quad (6)$$

where

$$\Phi(f_\tau,t)=-\frac{4\pi r_0}{c}Df_0+\pi K_m(t-\tau_d)^2-\frac{4\pi r_0}{c}\Phi_3(f_\tau)K_m^3(t-\tau_d)^3 \quad (7)$$

The delay time τ_d in Doppler-time domain is expressed as

$$\tau_d=\frac{2r_0}{cD} \quad (8)$$

and

$$K_m=\frac{K_r}{1+\frac{4\Phi_2(f_\tau)r_0K_r}{c}} \quad (9)$$

K_m can be approximately formulated as a linear function of the delay time τ_d at the reference range r_{ref}, which is generally chosen as the closest slant range from the scene center to the receiver [1, 16, 17]

$$K_m\approx K_{mref}+K_s(\tau_d-\tau_{dref})=K_{mref}+K_s\Delta\tau \quad (10)$$

where

$$\begin{cases} K_{mref}=\dfrac{K_r}{1+\frac{4\Phi_2(f_\tau)r_{ref}K_r}{c}} \\ \tau_{dref}=\dfrac{2r_{dref}}{cD} \\ K_s=-\dfrac{\mu^2}{2f_0D^2}K_{mref}^2 \end{cases} \quad (11)$$

2.2. Perturbation Function Multiplication

A Perturbation Function Multiplication (PFM) is carried out in the Doppler-time domain to remove the range-variance of second order

range terms, with a perturbation function consisting of second-order and third-order range time variables which is expressed as

$$H_{PFM}\left(f_\tau,t\right)=\exp\left\{j\left[\pi\gamma\left(f_\tau\right)\left(t-\tau_{ref}\right)^2-2\pi\xi\left(f_\tau\right)\left(t-\tau_{ref}\right)^3\right]\right\} \quad (12)$$

The residual phase after PFM operation is expressed as

$$\begin{aligned}\Phi_P\left(f_\tau,t\right)=&\frac{4\pi r_0}{c}Df_0+\pi\left[K_m\left(t-\tau_d\right)^2+\gamma\left(f_\tau\right)\left(t-\tau_{ref}\right)^2\right]\\&-2\pi\left[\frac{2r_0}{c}K_m^3\Phi_3\left(f_\tau\right)\left(t-\tau_d\right)^3+\xi\left(f_\tau\right)\left(t-\tau_{ref}\right)^3\right]\end{aligned} \quad (13)$$

The Perturbation coefficients $\gamma(f_\tau)$ and $\xi(f_\tau)$ will be determined in 2D frequency domain.

2.3. Range Fourier Transform

Applying Fourier Transform (FT) to the signal with respect to the range time variable t, via stationary point principle, and neglecting the contribution of the third-order terms in the point of stationary phase, we achieve,

$$G_P(f_\tau,f)=\sigma\left(\tau_0,r_0\right)\exp\left[j\Phi_P\left(f_\tau,f\right)\right] \quad (14)$$

where

$$\begin{aligned}\Phi_P\left(f_\tau,f\right)=&A_1\left(f_\tau,f\right)+A_2\left(f_\tau,f\right)\Delta\tau f+A_3\left(f_\tau,f\right)\Delta\tau f^2\\&+A_4\left(f_\tau,f\right)\Delta\tau^2 f+A_5\left(f_\tau,f\right)+2\pi f_\tau\tau_0\end{aligned} \quad (15)$$

$$\begin{cases}A_1\left(f_\tau,f\right)=-2\pi f\tau_{dref}-\pi\cdot\dfrac{f^2}{K_{mref}+\gamma}\\\qquad\qquad-\left(\dfrac{4\pi r_{ref}}{c}\Phi_3\cdot K_{mref}^3+2\pi\xi\right)\cdot\left(\dfrac{1}{K_{mref}+\gamma}\right)^3\cdot f^3\\A_2\left(f_\tau,f\right)=-\dfrac{K_{mref}}{2\pi D\left(K_{mref}+\gamma\right)}\\A_3\left(f_\tau,f\right)=-\left(\dfrac{4\pi r_0}{c}\Phi_3\cdot 3\gamma^2+2\pi\xi\right)\cdot\left(\dfrac{1}{K_{mref}+\gamma}\right)^3\cdot K_{mref}^2\\\qquad\qquad-2\pi\left(\dfrac{1}{K_{mref}+\gamma}K_s-\dfrac{K_s}{\left(K_{mref}+\gamma\right)^2}K_{mref}\right)\\A_4\left(f_\tau,f\right)=\pi\dfrac{K_s}{\left(K_{mref}+\Phi_2\right)^2}+\dfrac{4\pi r_0}{c}\Phi_3\cdot 3\gamma\cdot\left(\dfrac{1}{K_{mref}+\gamma}\right)^3\cdot K_{mref}^3\\\qquad\qquad-6\pi\xi K_{mref}\cdot\left(\dfrac{1}{K_{mref}+\gamma}\right)^3\\A_5\left(f_\tau,f\right)=\dfrac{\pi K_{mref}\gamma}{K_{mref}+\xi}\left[\dfrac{\pi K_s\gamma^2\Delta\tau^2}{\left(K_{mref}+\xi\right)^2}+\left(\dfrac{4\pi r_{ref}}{c}\Phi_3\gamma^3-2\pi\xi\right)\right.\\\qquad\qquad\left.\left(\dfrac{1}{K_{mref}+\xi}\right)^3K_{mref}^3\Delta\tau^3\right]\end{cases} \quad (16)$$

In order to remove the range-variance of the second- and third-order terms, $\gamma(f_\tau)$ and $\xi(f_\tau)$ should be chosen so the coefficient of $\Delta\tau f^2$ and $\Delta\tau^2 f$ are equal to zero, i.e.,

$$A_3(f_\tau, f) = 0, \quad A_4(f_\tau, f) = 0 \tag{17}$$

Solving (18) and (17) for $\gamma(f_\tau)$ and $\xi(f_\tau)$, we obtain

$$\begin{cases} \gamma(f_\tau) = \frac{c\Phi_2 K_{mref}}{3r_{ref}\Phi_1\Phi_3 - c\Phi_2} \\ \xi(f_\tau) = r_{ref}\Phi_2\Phi_3 K_{mref}^2 \left(\frac{2K_{mref}-1}{3r_{ref}\Phi_1\Phi_3 - c\Phi_2}\right) \end{cases} \tag{18}$$

Thus, the residential phase term $\Phi_P(f_\tau, f)$ is expressed as

$$\Phi_P(f_\tau, f) = A_1(f_\tau, f) + A_2(f_\tau, f)\Delta\tau f + A_5(f_\tau, f) + 2\pi f_\tau \tau_0 \tag{19}$$

2.4. Reference Function Multiplication

A Reference Function Multiplication (RFM) is readily performed to remove all the range-invariant phase, which is expressed as

$$H_{RFM}(f_\tau, f) = \exp\left[j\Phi_{RFM}(f_\tau, f)\right] \tag{20}$$

where

$$\Phi_{RFM}(f_\tau, f) = 2\pi\tau_{dref} f + \frac{\pi}{K_{mref} + \gamma} f^2 + \left(\frac{4\pi r_{ref}}{c}\Phi_3 \cdot K_{mref}^3 + 2\pi\xi\right) \cdot \left(\frac{1}{K_{mref} + \gamma}\right)^3 \cdot f^3 \tag{21}$$

The signal after RFM operation is expressed as

$$G_R(f_\tau, f) = \exp\left\{j\left[-\frac{K_{mref}}{2\pi D(K_{mref} + \gamma)}\Delta\tau f + A_5(f_\tau, f) + 2\pi f_\tau \tau_0\right]\right\} \tag{22}$$

2.5. Inverse Chirp-Z Transform

The ICZT operation is ready to be carried out to compensate the range-variant range cell migration phase by correcting the scaling factor in the range direction,

$$G_{ICZT}(f_\tau, t) = \int G_R(f_\tau, f) \cdot H(f_\tau, f, t)\, df \tag{23}$$

The new kernel for this operation is expressed as

$$H(f_\tau, f, t) = \exp(-j2\pi\beta f t) = \exp\left\{j\pi\beta\left[(f-t)^2 - f^2 - t^2\right]\right\} \tag{24}$$

where

$$\beta = -\frac{K_{mref}}{2\pi D^2(K_{mref} + \gamma)} \tag{25}$$

Thus (23) can be reformulated as

$$G_{ICZT}(f_\tau, t) = \exp\left(-j\pi\beta t^2\right) \int G_{RFM}(f_\tau, f) \exp\left(-j\pi\beta f^2\right) \exp\left[-j\pi\beta\left(f-t\right)^2\right] df \quad (26)$$

Thus the ICZT operation can be carried out through one convolution and two multiplications, as shown in Figure 2. The signal after ICZT is in Range-Doppler (RD) domain which is expressed as,

$$G_{ICZT}(f_\tau, t) = \sigma\left(\tau_0, r_0\right) p_r\left(t - \frac{2\left(r_0 - r_{ref}\right)}{c}\right) \exp\left[-j\left(A_5(f_\tau) - 2\pi f_\tau \tau_0\right)\right] \quad (27)$$

where $p_r(t)$ is the sinc-like pulse envelope in the range direction. From (27) we can see the scaling factor is equalized to be unity after ICZT operation.

2.6. Azimuth Residual Phase Compensation

Then azimuth residual phase compensation can be accomplished by multiplying (27) with a function which is formulated as

$$H_A(f_\tau, r_0) = \frac{\pi K_{mref}\gamma}{K_{mref} + \xi}\left[\frac{\pi K_s \gamma^2 \Delta\tau^2}{\left(K_{mref} + \xi\right)^2} + \left(\frac{4\pi r_{ref}}{c}\Phi_3\gamma^3 - 2\pi\xi\right)\left(\frac{1}{K_{mref} + \xi}\right)^3 K_{mref}^3 \Delta\tau^3\right] \quad (28)$$

The signal after the azimuth residual phase compensation is expressed as

$$G_A(f_\tau, t) = \sigma\left(\tau_0, r_0\right) p_r\left(t - \frac{2\left(r_0 - r_{ref}\right)}{c}\right) \exp\left(-j2\pi f_\tau \tau_0\right) \quad (29)$$

2.7. Inverse Fourier Transform

Performing IFT in azimuth to transform the data into the complex image domain yields

$$g\left(t, \tau\right) = \sigma\left(\tau_0, r_0\right) p_a\left(\tau - \tau_0\right) p_r\left(t - \frac{2\left(r_0 - r_{ref}\right)}{c}\right) \quad (30)$$

where $p_a(\tau)$ is the sinc-like compressed pulse envelope in the azimuth direction.

3. ANALYSIS AND COMPARISON

The proposed EICZT approach conquered the limitation of conventional ICZT by introducing a perturbation function to deal with the range-variance of second-order range terms, which is essential in high squint cases. In broadside configurations or low squint configurations, the proposed EICZT will also stand and provide improved quality, but may not be highly necessary, since in these cases the conventional ICZT can focus the signal well and simultaneously save one step (i.e., PFM operation). In this section, we will carry out analyses about the phase error to identify when the conventional ICZT starts to fail. Furthermore, experiments will be carried out to highlight the validation and essentiality of paying attention to the second and third-order terms.

As aforementioned, ICZT only takes the first order term into account, thus the phase error of ICZT algorithm Φ_{eICZT} is expressed as

$$\Phi_{eICZT} = -\frac{4\pi\left(r_0 - r_{ref}\right)}{c}\left\{\sqrt{(f_0+f)^2 - \left(\frac{cf_\tau}{2v}\right)^2} - \left[Df_0 + \Phi_1(f_\tau)f\right]\right\} \quad (31)$$

Practically, the acceptable level of maximum phase error is $\pi/4$, which means if the absolute value of Φ_{eICZT} ever exceeds $\pi/4$, the conventional ICZT will result in significant degradation of the image quality. As shown in (31), the phase error is determined by the swath width, the carrier frequency, the platform velocity and most importantly squint angle θ, because the squint angle will affect the azimuth frequency variable by shifting the Doppler Centroid by $2vf_0 \sin\theta/c$ [1]. An airborne experiment system is designed to show the influence of the squint angle to the phase error. The system parameters are listed in Table 1. The maximum phase error of ICZT algorithm with a squint angle from 0° to 60° is shown in Figure 3(a). From the image we can see, the phase error is acceptable when the squint angle is smaller than 30°, but when the squint angle exceeds 30°, ICZT will seriously degrade the focusing performance. The critical point will be smaller with the increase of swath width.

However, the proposed EICZT algorithm brings the accuracy up to the third order, then the phase error becomes

$$\Phi_{eEICZT} = -\frac{4\pi r_0}{c}\left\{\sqrt{(f_0+f)^2 - \left(\frac{cf_\tau}{2v}\right)^2} - \left[Df_0 + \Phi_1(f_\tau)f + \Phi_2(f_\tau)f^2 + \Phi_3(f_\tau)f^3\right]\right\} \quad (32)$$

Table 1. System parameters.

Platform velocity	150 m/s
Azimuth antenna length	1 m
Platform altitude	10000 m
Squint angle	0∼60°
Depression angle	45°
Carrier frequency	10 GHz
PRF	500 Hz
Swath Width	3000 m
Range bandwidth	300 MHz

Figure 3(b) shows the maximum phase error of EICZT algorithm with the squint angle from 0° to 60°. The phase error is approximately equal to zero, which indicates that the proposed EICZT approach can provide satisfying accuracy in high squint configuration and the additional PFM operation is highly indispensable.

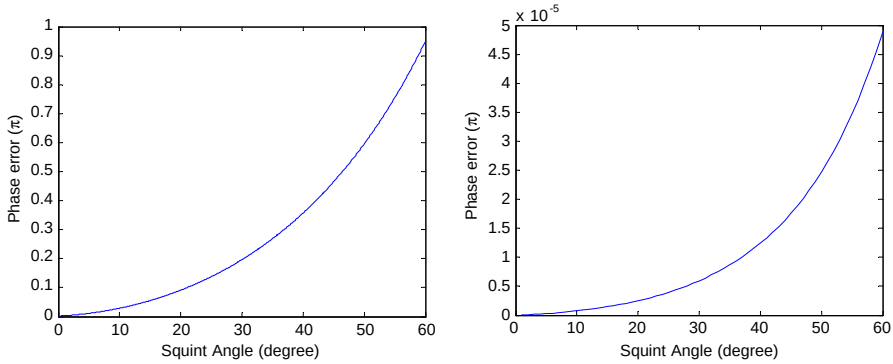

Figure 3. Phase error variation with the increase of squint angle for (a) conventional ICZT, (b) the proposed EICZT.

4. SIMULATION EXPERIMENTS AND REAL DATA PROCESSING RESULTS

A high-squint airborne simulation with a squint angle of 40° is carried out in this section to highlight the performance of proposed algorithm.

The designed scene consists of nine point targets, as shown in Figure 4. PT5 locates at the scene center, the near range and far range targets have a relative slant range of −1500 m and 1500 m. The distance between PT2 and PT5 is 1000 m in azimuth. For the ongoing simulations, we assume the window function of rectangular shape in both directions. The system parameters are shown in Table 1. The theoretical azimuth resolution and range resolution are 0.65 m and 0.5 m, respectively. In this configuration, the maximum phase error of conventional ICZT is higher above the acceptable level $\pi/4$, as shown in Figure 5(b), and the phase error of EICZT remains to be approximately zero, as shown in Figure 5(a).

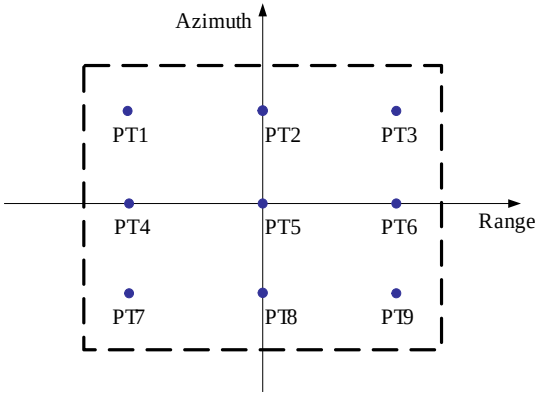

Figure 4. Scene geometry with nine point targets.

For clarity, the two-dimensional impulse response of PT1 focused by the proposed approach is zoomed in and shown in Figure 5(c). To quantify the precision of processing, the impulse response width (IRW), peak sidelobe ratio (PSLR), and integrated sidelobe ratio (ISLR) are used as criteria, as listed in Table 2. From Table 2, it can be seen that the measured IRWs processed by using EICZT in range and azimuth agree well with the theoretical values of 0.65 m in azimuth and 0.5 m in range, as shown in Table 2. However, the measured IRWs processed by using conventional ICZT are broadened by a factor of 22% and 47% in range and azimuth, as shown in Figure 5(d). Therefore, it means that the proposed EICZT approach is essential and capable of focusing SAR data in the high-squint configuration and highly improves the image quality with respect to the conventional ICZT.

For Further validation of the proposed signal processing approach, a set of real X-band SAR data acquired by an airborne SAR system is used. The system bandwidth is 330 MHz, the pulse repetition

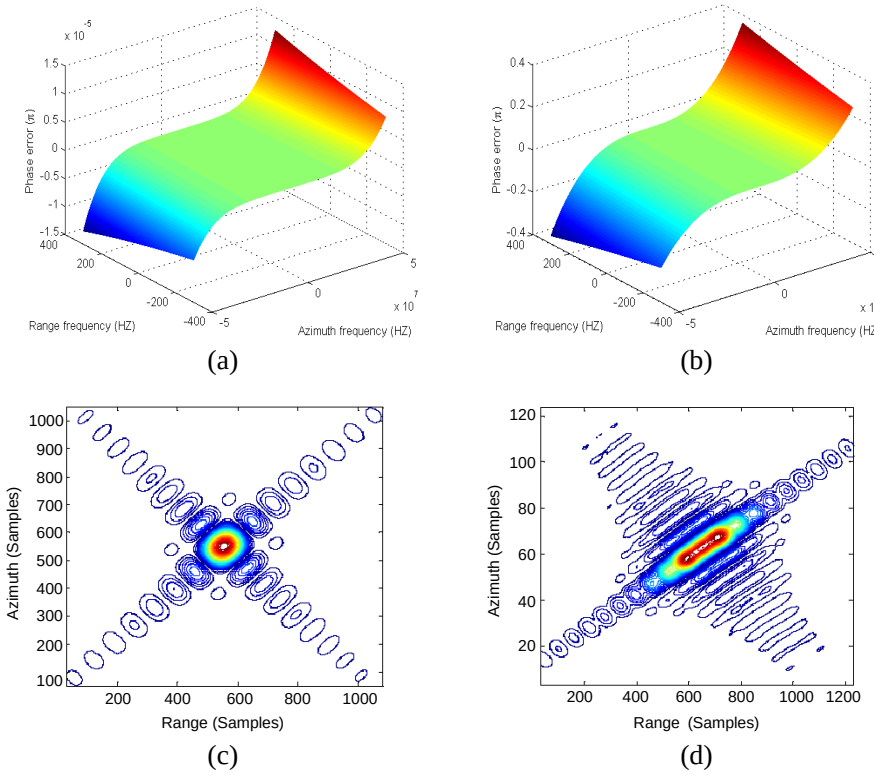

Figure 5. (a) Phase error of the proposed EICZT with 40° squint angle. (b) Phase error of conventional ICZT with 40° squint angle. (c) Impulse response of PT1 focused by the proposed algorithm. (d) Impulse response of PT1 focused by conventional ICZT.

Table 2. Parameters of focused targets.

	Azimuth			Range		
	IRW	**PSLR**	**ISLR**	**IRW**	**PSLR**	**ISLR**
EICZT	0.65 m	−13.22 B	−9.82 dB	0.501 m	−13.23 B	−9.86 dB
ICZT	0.96 m	−8.89 B	−12.32 dB	0.61 m	−9.23 B	−12.16 dB

frequency is 1600 Hz, and the velocity of the airplane is 140 m/s. To achieve accurate focusing, the onboard Inertial Navigation System (INS) and the Global Positioning System (GPS) are used to collect the information of the position and attitude of the antenna phase center.

In this paper, we choose the slant range at the middle swath as

Figure 6. SAR image processed by the proposed approach. The horizontal and vertical directions denote the range and azimuth, respectively.

the reference range. By using the proposed imaging algorithm, the outcoming SAR image is shown in Figure 6.

5. CONCLUSION

The traditional ICZT can focus broadside or low squint SAR data well, but fail in high squint configurations due to the neglect of range-variance of the second order range terms. The EICZT approach is proposed in this paper with a pre-processing operation in the Doppler-time domain by formulating a perturbation function to compensate the range-variance of second order range terms, which makes ICZT capable to work in high squint configurations. The simulated high squint SAR targets are well focused by the proposed processing approach and show great improvement with respect to the ones focused by conventional ICZT. The processing result of the real SAR data proves that the proposed EICZT approach can work well in the case of the millimeter-wave SAR. Due to the ability of this proposed algorithm, it can be capable of working in the spaceborne high-resolution sliding spotlight, and spaceborne high squint configurations.

REFERENCES

1. Cumming, I. G. and F. H. Wong, *Digital Processing of Synthetic Aperture Radar Data Algorithms and Implementation,* Artech

House, Norwood, MA, 2005.

2. Ender, J. H. G. and A. R. Brenner, "PAMIR: A wide-band phased array SAR/MTI system," *IEE Proc. — Radar Sonar Navig.*, Vol. 150, No. 3, 165–172, 2003.
3. Liu, Q., W. Hong, W. X. Tan, Y. Lin, Y. Wang, and Y. Wu, "An improved polar format algorithm with performance analysis for geosynchronous circular SAR 2D imaging," *Progress In Electromagnetics Research*, Vol. 119, 155–170, 2011.
4. Wei, X., P. Huang, and Y. K. Deng, "Multi-channel SPCMB-TOPS SAR for high-resolution wide-swath imaging," *Progress In Electromagnetics Research*, Vol. 116, 533–551, 2011.
5. Buddendick, H. and T. F. Eibert, "Bistatic image formation from shooting and bouncing rays simulated current distributions," *Progress In Electromagnetics Research*, Vol. 119, 1–18, 2011.
6. Banasiak, R., R. Wajman, D. Sankowski, and M. Soleimani, "Three-dimensional nonlinear inverstion of electrical capacitance tomography data using a complete sensor model," *Progress In Electromagnetics Research*, Vol. 100, 219–234, 2010.
7. Park, J.-I. and K.-T. Kim, "A comparative study on ISAR imaging algorithms for radar target identification," *Progress In Electromagnetics Research*, Vol. 108, 155–175, 2010.
8. Chang, Y. L., C. Y. Chiang, and K. S. Chen, "SAR image simulation with application to target recognition," *Progress In Electromagnetics Research*, Vol. 119, 35–57, 2011.
9. Zhang, M., Y. W. Zhao, H. Chen, and W. Q. Jiang, "SAR imaging simulation for composite model of ship on dynamic ocean scene," *Progress In Electromagnetics Research*, Vol. 113, 395–412, 2011.
10. Zhao, Y. W., M. Zhang, and H. Chen, "An efficient ocean SAR raw signal simulation by employing fast Fourier transform," *Journal of Electromagnetic Waves and Applications*, Vol. 24, No. 16, 2273–2284, 2010.
11. Wei, S. J., X. L. Zhang, and J. Shi, "Linear array SAR imaging via compressed sensing," *Progress In Electromagnetics Research*, Vol. 117, 299–319, 2011.
12. Bamler, R., "A comparison of range-Doppler and wavenumber domain SAR focusing algorithm," *IEEE Trans. Geosci. Remote Sens.*, Vol. 40, No. 4, 706–713, Jul. 1992.
13. Davidson, G. W., I. G. Cumming, and M. R. Ito, "A chirp scaling approach for processing squint mode SAR data," *IEEE Trans. Aerosp. Electron. Syst.*, Vol. 32, No. 1, Jan. 1996.
14. Cantalloube, H. and P. Dubois-Fernandez, "Airborne X-band

SAR imaging with 10 cm resolution: Technical challenge and preliminary results," *IEE Proc. — Radar Sonar Navig.*, Vol. 153, No. 2, 173–176, Apr. 2006.

15. Jin, Y.-Q., "Polarimetric scattering modeling and information retrieval of SAR remote sensing — A review of FDU work," *Progress In Electromagnetics Research*, Vol. 104, 333–384, 2010.
16. Wong, F. H. and T. S. Yeo, "New applications of nonlinear chirp scaling in SAR data processing," *IEEE Trans. Geosci. Remote Sens.*, Vol. 39, No. 5, 946–953, May 2001.
17. Mittermayer, J., A. Moreira, and O. Loffeld, "Spotlight SAR data processing using the frequency scaling algorithm," *IEEE Trans. Geosci. Remote Sens.*, Vol. 37, No. 9, 2198–2214, Sep. 1999.
18. Liu, Y., Y. Deng, R. Wang, and X. Jia, "Bistatic FMCW SAR raw signal simulatior for extended scenes," *Progress In Electromagnetics Research*, Vol. 128, 479–502, 2012.
19. Natroshvili, K., O. Loffeld, H. Nies, A. M. Ortiz, and S. Knedlik, "Focusing of general bistatic SAR configuration data with 2-D inverse scaled FFT," *IEEE Trans. Geosci. Remote Sens.*, Vol. 44, No. 10, 2718–2727, Oct. 2006.
20. Rabiner, L. R., R. W. Schafer, and C. M. Rader, "The chirp-Z transform and its applications," *IEEE Trans. Audio. Electro.*, Vol. 17, No. 2, 86–92, Jun. 1969.
21. Tang, Y., M. D. Xing, and Z. Bao, "The polar format imaging algorithm based on double chirp-Z transforms," *IEEE Geosci. Remote Sens. Lett.*, Vol. 5, No. 4, 610–614, Oct. 2008.
22. Lanari, R., S. Hensley, and P. A. Rosen, "Chirp Z-transform based SPECAN approach for phase-preserving ScanSAR image generation," *IEE Proc. — Radar Sonar Navig.*, Vol. 145, No. 5, Oct. 1998.
23. Lanari, R. and G. Fornaro, "A short discussion on the exact compensation of the SAR range-dependent range cell migration effect," *IEEE Trans. Geosci. Remote Sens.*, Vol. 35, No. 6, 1446–1451, Nov. 1997.
24. Lanari, R., "A new method for the compensation of the SAR range cell migration based on the chirp Z-transform," *IEEE Trans. Geosci. Remote Sens.*, Vol. 33, No. 5, 1296–1299, Sep. 1995.